Engineering materials properties in codimension > 0

Paulo S. Branicio, Mark H. Jhon, and David J. Srolovitz[a)]
Institute of High Performance Computing, Singapore 138632, Singapore

(Received 3 June 2011; accepted 26 August 2011)

When thin nanomaterials spontaneously deform into nonflat geometries (e.g., nanorods into nanohelices, thin sheets into ruffled forms), their properties may change by orders of magnitude. We discuss this phenomenon in terms of a formal mathematical concept: codimension $c = D - d$, the difference between the dimensionality of space D, and that of the object d. We use several independent examples such as the edge stress of graphene nanoribbons, the elastic moduli of nanowires, and the thermal expansion of a modified bead-chain model to demonstrate how this framework can be used to generically understand some nanomaterial properties and how these properties can be engineered by using mechanical constraints to manipulate the codimension of the corresponding structure.

I. INTRODUCTION

Low-dimensional nanomaterials such as carbon nanotubes (CNTs),[1,2] nanowires,[3,4] and graphene[5] have properties that are very different from bulk materials. Although these properties are usually attributed to their high surface area to volume ratio or quantum confinement effects, these materials are distinct from the bulk in another important way. Low-dimensional nanostructures can be flexible and may not be straight/flat at equilibrium. These shapes arise because of a compromise between bending energy and other forces, for example, surface stress, internal stress, electrostatic interaction, or adsorption. There are myriad examples of such nanostructures, including ZnO and SnO_2 nanobelts,[6,7] graphene nanoribbons (GNRs),[8] silica/carbonate helicoids,[9] SiGe nanodrills,[10] and SiGe/Si/Cr nanocoils.[11]

Because thermodynamic properties are defined relative to an *equilibrium state*, the properties of a nanostructure will depend on the shape of that structure. Although these shapes are not unique to the nanometer scale, they are more common in nanostructures because of the strong influence of surfaces and low mechanical rigidity. This observation leads us to classify nanostructures based on the number of dimensions into which they can spontaneously deform c. Formally, c is the codimension of the nanostructure: the difference between the dimensionality of the space in which the material is embedded D (i.e., in which it can deform), and the intrinsic dimensionality of the object d.[12,13] The codimension is a measure of the spatial degrees of freedom of the nanostructure. For example, a graphene sheet and a nanowire embedded in a three-dimensional space has codimension $c = 3 - 2 = 1$ and $c = 3 - 1 = 2$, respectively. If a nanowire, in three dimensions, is constrained to remain straight (i.e., it is prevented from deforming into the other two dimensions), it has codimension $c = 1 - 1 = 0$.

The properties of a nanostructure can be distinct from the properties of the corresponding bulk material. The thermodynamic properties of a nanostructure are defined relative to *nanoscale* variables. For example, for a nanowire, we may be interested in the application of a mechanical load along its axis. Two relevant thermodynamic variables are the length of the nanowire and the force on the ends of the nanowire. Obviously, if a flexible nanostructure bends rather than stretches, it will appear to have a very small stiffness. In other words, the thermodynamic properties of the nanostructure depend on *how the material deforms*. In contrast, bulk thermodynamic quantities, such as the Young's modulus, are defined relative to the microscopic strain state of a volume element.

This study examines how a flexible, low-dimensional nanostructure with $c = D - d > 0$ can have very different properties than the same material in $c = 0$. In $c = 0$, structures will be "bulklike," whereas in $c > 0$, their shape may be important. We further propose that for low-dimensional, flexible objects, these c-dependent properties may be engineered by introducing interactions with a stiff substrate. In the following sections, we discuss three examples of how codimension affects properties. We first illustrate this idea using a "toy" model for thermal expansion of a flexible material. Then, we discuss the c dependence of the stiffness of nanowires and the edge energy and edge stress of GNRs.

II. THERMAL EXPANSION OF A BEAD CHAIN IN $c \geq 0$

In order to illustrate the generic relationship between codimension and materials properties, we consider a model system of a chain of N beads connected by linear springs of stiffness k and equilibrium length a_0 at $T = 0$.

a)Address all correspondence to this author.
e-mail: srol@ihpc.a-star.edu.sg
DOI: 10.1557/jmr.2011.306

 © Materials Research Society 2011

https://doi.org/10.1557/jmr.2011.306 Published online by Cambridge University Press

The position of the ith bead is described by $\mathbf{r}_i$. This geometry is illustrated in Fig. 1. At any finite temperature, a bead chain will tend to *crumple* into a compact (rather than linear) configuration because of its lack of bending rigidity. To prevent crumpling, the chain can be placed in a strong external potential $\gamma x_i^2/2$, where γ is the interaction strength and x_i is the displacement of the ith bead perpendicular to the nominal chain axis. This potential penalizes deformations out of the chain-line direction (z in this example, Fig. 1). We analyze this model for cases where beads can move in different codimensions, and we find that the sign of the coefficient of thermal expansion (CTE) is determined by the codimension of the space.

In $D = 2$ ($c = 1$), the potential energy of this system is written as

$$U = \sum_i \left[\frac{1}{2}k(|\mathbf{r}_i - \mathbf{r}_{i-1}| - a_0)^2 + \frac{1}{2}\gamma x_i^2\right] \quad , \qquad (1)$$

where $\mathbf{r}_i = (x_i, z_i + ia)$ and a is the lattice constant of the system at the temperature of interest. We consider this model in the limit that the vibrations of the beads are small compared to a. In this limit ($a \gg |\mathbf{r}_i - \mathbf{r}_{i-1}|$, for all i), we may linearize U as

$$U = \sum_i \left[\frac{k}{2a}(a - a_0)(x_i - x_{i-1})^2 + \frac{1}{2}\gamma x_i^2 + \frac{1}{2}k[z_i - z_{i-1} - (a - a_0)]^2\right] \quad . \qquad (2)$$

We calculate a rigorous upper bound for the Helmholtz free energy $A(T, L)$ using the Gibbs–Bogoliubov inequality,

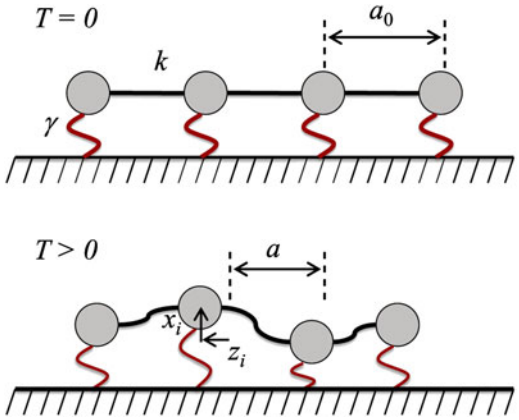


FIG. 1. A modified bead-chain model is illustrated at $T = 0$ and at $T > 0$. The beads are connected to each other by springs with harmonic constant k and are connected to the substrate with springs with harmonic constant γ. Here, a_0, the equilibrium lattice constant at $T = 0$, is in general different from a, the average lattice spacing at $T > 0$. The position of the ith atom is described relative to a crystalline lattice using the displacements x_i and z_i.

$$A \leq A_0 + \langle U - U_0\rangle_0 \quad , \qquad (3)$$

where the free energy and potential energy of a reference state are A_0 and U_0, respectively. Following the methods of LeSar et al.[14] and Mansoori et al.,[15] we perform a variational calculation, choosing the reference state to be an Einstein solid with lattice parameter a. In this case, the probability of finding a bead displacement (x_i, z_i) is described by a Gaussian function centered around a lattice site, $\sqrt{\alpha_x\alpha_z}/\pi \exp\left(-\alpha_x x_i^2 - \alpha_z z_i^2\right)$, where α_x and α_z are constants. The A_0 for this Einstein solid is

$$A_0 = \frac{Nk_BT}{\pi}\ln\left(\Gamma^2\sqrt{\alpha_x\alpha_z}\right) \quad , \qquad (4)$$

where Γ is the thermal wavelength and N is the number of beads. The expression $\langle U\rangle_0$ is found by averaging U over the Gaussian functions,

$$\langle U\rangle_0 = k\frac{\alpha_x + \Delta(1 + \Delta a^2\alpha_x)\alpha_z}{2\alpha_x\alpha_z} + \frac{\gamma}{4\alpha_x} \quad , \qquad (5)$$

where $\Delta = (a - a_0)/a$. According to the equipartition theorem, $\langle U_0\rangle_0 = Nk_BT$. We can approximate A by optimizing $A_0 + \langle U - U_0\rangle_0$ with respect to a. Next, we determine the CTE in arbitrary codimension $c = D - 1$ by taking the appropriate derivative of the free energy:

$$\text{CTE} = \frac{1}{a}\left(\frac{\partial a}{\partial T}\right) \approx -\frac{ck_B}{\gamma a_0^2} \quad . \qquad (6)$$

In order to test this result, we perform molecular dynamics on this modified bead-chain model. The molecular dynamics simulation was initialized by arranging all of the beads in a linear chain, with lattice spacing $a_0 = 3$ Å. The system is equilibrated at low temperatures using a NVT thermostat, and the lattice constant (mean spacing between beads) is measured as a function of the temperature. The results are presented in Fig. 2.

Figure 2 shows that the CTE $\to 0$ as $\gamma \to \infty$. This is because this model is purely harmonic. Very large values of γ imply that the chain is constrained to be linear, and so the effective codimension is $c_{\text{eff}} \approx 0$. Smaller values of γ imply more freedom to explore higher dimensions (i.e., weaker confinement) and greater deviations from $c = 0$. Here γ can be interpreted as a measure of mechanical constraint that continuously interpolates between $c = 0$ and the maximum codimension $c > 0$. Equation (6) is derived assuming strong confinement, in which $\gamma > 0$ (i.e., nearly straight). However, we note that at any finite temperature if a straight bead chain is under no confinement (not describable based on the perturbative approach of Eq. (6), then an entropic force will tend to bring the two ends together. If we take the reference state to be the fully extended chain at $T = 0$, the chain will always have a negative CTE.

https://doi.org/10.1557/jmr.2011.306 Published online by Cambridge University Press

Our bead-chain model qualitatively describes the behavior of nearly linear polymer chains, such as the polymer chains within CNTs that have recently been observed.[16–19] A polymer chain inside a very narrow CNT corresponds to $c_{\text{eff}} = 0$, because the confinement would constrain the polymer chain, severely restricting its displacements away from the CNT axis. McIntosh et al.[20] calculated the equilibrium distance between a polyacetylene chain and a CNT wall to be 3.3 Å. Based on their estimates a (4,4) and (5,5) arm chair CNT would provide strong confinement and have therefore $c_{\text{eff}} \approx 0$. In contrast for, wide CNTs, the confinement would the reduced, leading to $c_{\text{eff}} > 0$; for example, a (6,6), (7,7), or wider CNT is predicted to provide much less confinement and have therefore $c_{\text{eff}} > 0$. Other approachs to modify the c_{eff} of a polymer within a nanotube include stiffening the nanotube by going from single to multiwall tubes, increasing the diameter of the polymer chain by modification of the polymer side groups, and varying the number of polymer chains inside the CNT.

It is useful to compare our predictions to predictions for related systems. The present findings are consistent with the predicted low temperature behavior of graphene. Although the CTE of graphene is positive in $c = 0$ (i.e., the material is not perfectly harmonic), recent experiments show that the CTE of graphene in $c = 1$ is negative at low temperature and becomes positive at higher temperature.[21] This is consistent with our bead-chain results above and the calculations of Jiang et al.[22] However, if a strong substrate interaction is imposed ($c_{\text{eff}} \approx 0$), the CTE becomes positive at all temperatures.[22] Using the example of CTE, we have shown that properties can be tuned by appropriately changing the codimension. In the next section, we discuss the implications of codimension on other classes of properties.

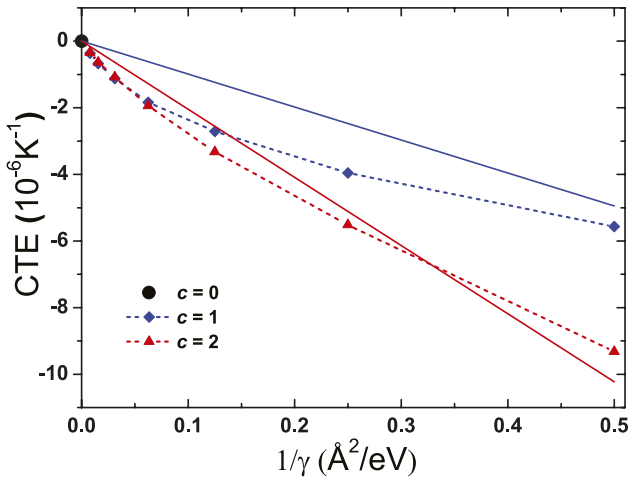


FIG. 2. CTE of a nominally linear chain of beads connected by harmonic springs as a function of the inverse confinement interaction strength $1/\gamma$ in codimensions $c = 0$, 1, and 2. Continuous solid lines show the analytical result and dotted lines connect molecular dynamics data points.

III. THE STIFFNESS OF A NANOWIRE IN $c \geq 0$

Another clear example of the effects of codimension on materials properties may be found in the dependence of the elastic response of a nanowire on its equilibrium shape. Consider the case of nanowires that, in equilibrium, exhibit a helical or springlike shape (i.e., nanohelices) as, for example, recent observations in ZnO,[6] SiC,[23] and SiGe/Si/Cr.[11] Because the nanohelix deforms in three dimensions upon application of a tensile load, it is a $c = 3 - 1 = 2$ structure; in contrast, a straight nanowire deforms in one dimension (i.e., $c = 1 - 1 = 0$). The stiffnesses of these two structures will be very different. In this section, we explicitly compare the elastic response of two nanowires, in a helical and straight (rod) form, with the same cross-sectional dimensions and same end-to-end distance L. Of course, a much greater force is required to stretch a straight nanorod to the same extent as a nanohelix.

The stiffness of a straight wire with end-to-end distance L and uniform cross section [see Fig. 3(a)] is calculated using Hooke's law,

$$M_{c=0} = \frac{EA}{L} \quad , \tag{7}$$

where E is the Young's modulus of the material and A is the cross-sectional area of the rod. In contrast, if the wire is

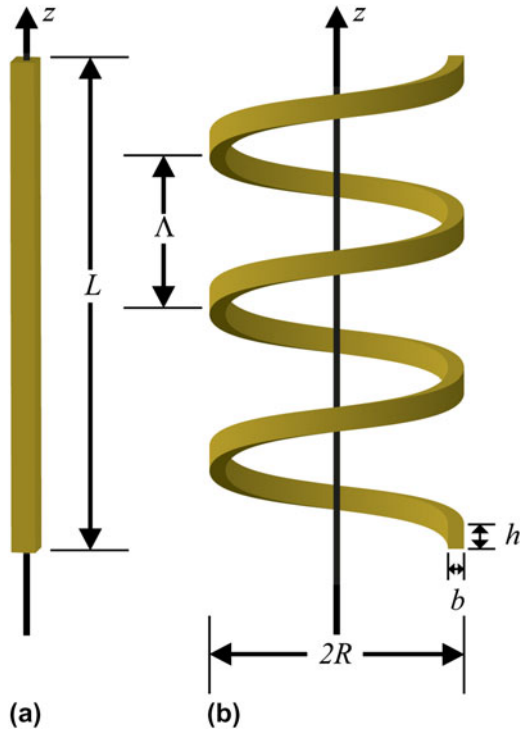


FIG. 3. (a) Schematic illustrations of a straight rod ($c = 0$) with a rectangular cross section and (b) a similar rod in an equilibrium helical spring configuration ($c = 2$). The relevant geometrical parameters defining the helical spring are the cross-section width (h) and thickness (b), the mean coil radius R, and the helix pitch Λ.

https://doi.org/10.1557/jmr.2011.306 Published online by Cambridge University Press

a helix, its stiffness can be calculated using standard mechanics methods,[24–26]

$$M_{c=2} = \frac{GJ\Lambda}{2\pi LR^3} \quad , \tag{8}$$

where L is the end-to-end length of the helix, R is the radius of the coil, Λ is the helix pitch, J is the torsion constant, and G is the shear modulus of the material, as illustrated in Fig. 3(b). If one bends a wire into a helix, it will have a shorter end-to-end length than the length L of the wire. The stiffness of this object can be calculated from Eq. (8) by scaling L by the geometrical factor $\Lambda/2\pi R$.

Comparing Eq. (7) and Eq. (8), we find that the spring constant of a helix relative to that of a rod with the same end-to-end length is reduced by a factor

$$\frac{M_{c=2}}{M_{c=0}} = \frac{\Lambda J}{4\pi(1-\nu)AR^3} \quad . \tag{9}$$

Using Eq. (9), we can predict the magnitude of the reduction in the spring constant of the ZnO nanohelices produced by Kong and Wang[6] relative to straight ZnO nanoribbons of the same length and cross section. For this case, the spring constant ratio is

$$\frac{M_{c=2}}{M_{c=0}} \approx 3 \times 10^{-6}, \tag{10}$$

where we have substituted the geometical parameters from the Kong and Wong[6] results (typical radii of $R = 500$ nm, pitch of $\Lambda = 150$ nm, and rectangular cross sections of $h \times b = 30 \times 10$ nm) and the torsion constant from Young and Budynas.[26] Note that there is an approximately 1 million times reduction in the force required to stretch a $c = 2$ nanohelix as compared with stretching a $c = 0$ straight nanorod to the same extension.

IV. THE EDGE ENERGY AND STRESS OF A GNR

Graphene is a nominally two-dimensional, flexible, model nanomaterial. It has attracted considerable theoretical and experimental attention since graphene sheets and GNRs were first fabricated.[5,27–29] In this section, we use codimension to reinterpret two important materials properties of graphene: the edge energy and the edge stress.

Recent theoretical studies found that graphene edges can exhibit large compressive edge stresses.[30–32] Empirical potential calculations have shown that in $c = D - d = 3 - 2 = 1$, this compressive stress can cause edge warping or GNR twisting,[8,33] in qualitative agreement with the elastic behavior of macroscopic plates.[34] Experiments have also shown that graphene and boron nitride nanoribbons can extensively bend and twist and have their edges rippled to accommodate the stress.[35,36]

The edge energy is given by

$$E_e(\epsilon) = \gamma_0 + \tau_e\epsilon + \ldots \quad , \tag{11}$$

where we have defined the edge stress τ_e as the energy cost required to deform a GNR edge by an infinitesimal strain ϵ parallel to the edge from the equilibrium configuration at $\epsilon = 0$.

In differential form,

$$\tau_e = \left(\frac{dE_e}{d\epsilon}\right)_{\epsilon=0} \quad . \tag{12}$$

Figure 4(a) shows a GNR that is constrained to $c = 0$ by restricting the sheet to $D = 2$. We determine the properties of this GNR and of several other GNRs for edge orientations between (and including) the well-studied armchair and zigzag orientations.[37] As indicated in Fig. 5(a) (atoms in local armchair/zigzag edge configurations are shown in orange/red), intermediate orientations contain segments of both the armchair and zigzag edge geometries.

We determine the equilibrium GNR structure at $T = 0$ by minimizing the total energy with respect to all atom coordinates using the reactive empirical bond order potential (REBO-II)[38] and imposing periodic boundary conditions along the GNR length. The edge energy E_e, determined in

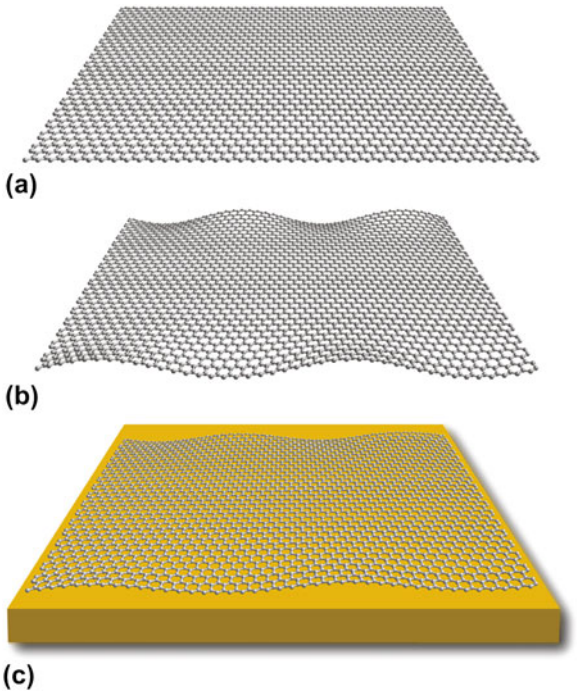


FIG. 4. GNRs illustrated in different codimensions c. (a) A flat GNR ($c = 0$) at $T = 0$. (b) The same GNR as in (a) that spontaneously deforms into a third dimension ($c = 1$). In this case, the compressive edge stresses lead to edge warping while the interior of the GNR remains flat. (c) A GNR interacting with a substrate resulting in an effective codimension c between (a) $c = 0$ and (b) $c = 1$. For this case the warping will have a lower magnitude than for (b).

https://doi.org/10.1557/jmr.2011.306 Published online by Cambridge University Press

this equilibrium configuration, is shown in Fig. 5(b). The edge stress τ_e for the relaxed GNRs is shown in Fig. 5(c) and is obtained from the slope of a plot of edge energy E_e versus uniaxial strain (parallel to the ribbon axis). Details of the calculation of edge energy and stress can be found in Appendix A. Both E_e and τ_e for the relaxed GNRs vary smoothly with orientation α, and E_e varies by less than 10% with edge angle α. In contrast, the variation of the edge stress τ_e with α is much larger (~50%). The magnitude of both quantities is in reasonable agreement with density functional theory[30–32,39] and empirical potential calculations.[33,39,40] The results shown in Fig. 5(b) closely follow the analytical expressions for the edge energy reported recently.[37,39]

When a GNR is embedded in three dimensions ($D = 3$) rather than two (i.e., the GNR is not constrained to be flat), the edges buckle in the direction normal to the GNR plane, producing the edge ripples seen in Fig. 4(b). The rippling or warping decays away from the edge toward the interior of the GNR, which remains nearly flat, in agreement with earlier simulations.[33]

The effect of codimension on GNR edge properties is illustrated in Fig. 5. The edge energy E_e changes very little with codimension. In contrast, the edge stress τ_e changes sign (goes from strongly compressive to slightly tensile) upon increasing the codimension from $c = 0$ to $c = 1$ (i.e., allowing relaxation into the orthogonal direction). These results show that although some properties (e.g., τ_e) change dramatically with codimension, other related properties (e.g., E_e) are nearly independent of c.

These results raise some questions. What edge stress would be measured in an experiment? Would it be the large $c = 0$ compressive stress or would it be the relaxed, tensile stress for $c = 1$? If a free-standing GNR of a length that is large compared to the edge rippling wavelength is stretched along its axis, clearly the edge stress would be $\tau_{c=1}$ not $\tau_{c=0}$. In contrast, if a GNR is strongly bonded to a substrate and the system is stretched in the same manner, the edge stress would be $\tau_{c=0}$ not $\tau_{c=1}$.

Intuitively, we can imagine that by applying a mechanical constraint to the graphene sheet, we can engineer the edge stress. A natural way to do this is to adsorb graphene onto a substrate. A recent experimental study by Lui et al.[41] in which graphene was deposited on flat mica surfaces showed that the resultant graphene sheets

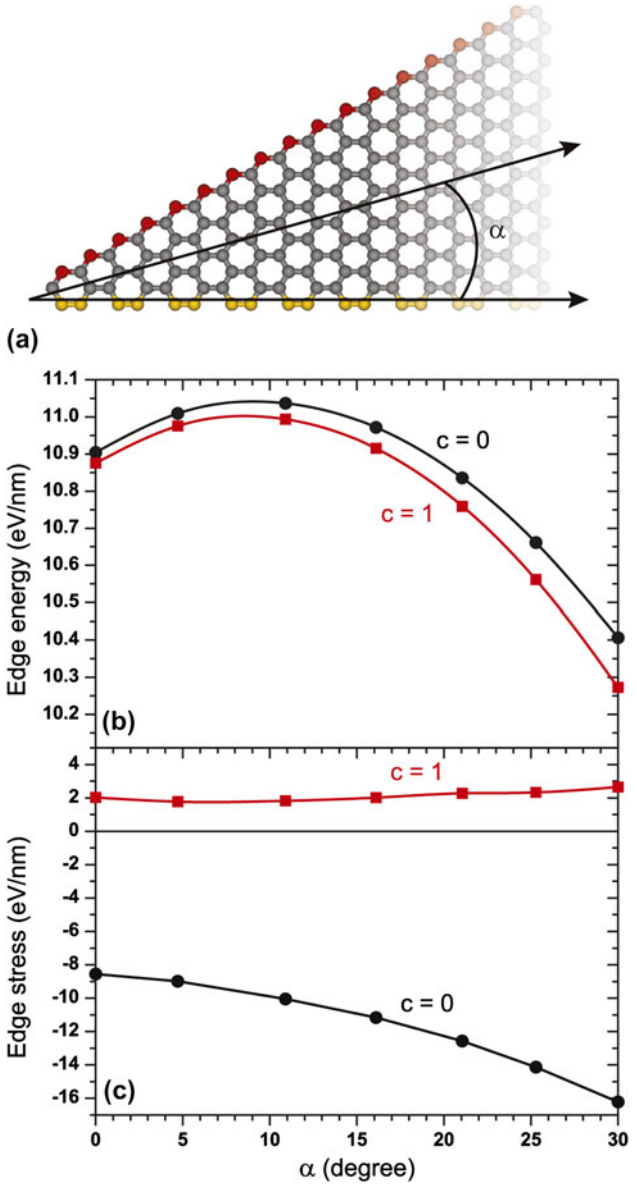


FIG. 5. Edge energies and stresses for arbitrary graphene edges. (a) The definition of the edge angle α with respect to a graphene sheet; $\alpha = 0°$ corresponds to the armchair edge (yellow) and $\alpha = 30°$ to the zigzag edge (red). (b) Graphene edge energy E_e as a function of edge angle $0° < \alpha < 30°$. Values are shown for $c = 0$ and 1. (c) Graphene edge stress τ_e for the same edges as in (b).

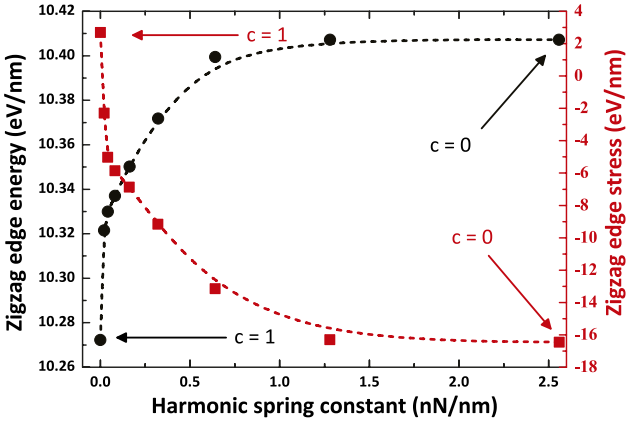


FIG. 6. Codimension dependence of graphene zigzag edge energy E_e and edge stress τ_e. The effective codimension varies from $c_{eff} = 0$ to $c_{eff} = 1$ by changing the strength of the harmonic interaction γ with a rigid substrate. Although these results are for the zigzag edge, similar dependences are found for the other edge orientations.

https://doi.org/10.1557/jmr.2011.306 Published online by Cambridge University Press

were ultraflat compared with free or suspended graphene. By controlling the chemical nature of the surface it would be possible to modify the degree of constraint that would accompany that adsorption of graphene. For example, free standing graphene would correspond to $c = 1$, graphene on a gold substrate to $c = 0$, but graphene on a gold substate on which thiols were chemisorbed prior to graphene adsorption would lead to a relatively weak constraint of the graphene, yielding an effective codimension $0 < c_{\text{eff}} < 1$ [see Fig. 4(c)].

We investigate this possibility by modeling the interaction of graphene with a substrate and its effect on edge properties by introducing a harmonic potential $\frac{1}{2}\gamma u_z$ that penalizes out-of-plane deformation. We then recalculate the edge stress as a function of γ. As shown in Fig. 6, the edge stress τ_e varies rapidly with the strength of the bonding to the substrate, but the edge energies E_e show only a very weak dependence on the strength of the bonding γ. This reinforces our earlier conclusions on the effect of codimension on GNR edge properties.

V. DISCUSSION

We have demonstrated, through a disparate series of examples, that low-dimensional materials have properties that can be strongly dependent on the dimensionality of the space in which they "live." This peculiar condition is captured by the broad codimension concept. This can be related to two other very important, general principles. First, codimension is quite similar to the degree of freedom concept. The codimension dictates the *geometrical* degrees of freedom that a low dimensional material can access. However, these degrees of freedom are *not arbitrary*, but are instead determined by the flexibility of the structure. Second, codimension is a generalization of the concept of mechanical constraint. Constraint is typically only applied to mechanical properties, but we have shown that it can be applied more broadly, such as to thermal expansion.

This discussion allows us to speculate on the types of properties that are likely to be highly c-dependent. Because of the increased degrees of geometric freedom, bending and twisting in nanostructures breaks the local crystal symmetry. This changes the symmetry constraints on equilibrium properties and can make such properties sensitive to codimension changes. Consider the spontaneous polarization of a ferroelectric nanohelix, such as ZnO. Even if the dipole moment of each unit cell does not change on going from the bulk to a nanowire geometry, the spontaneous polarization will change dramatically with the radius and pitch of the equilibrium helical structure. Similarly, the piezoelectric constants of a nanohelix will be much reduced compared with when the same material is a straight nanorod. In general, deformation into higher dimensions will have a small effect on properties that are determined largely by point group symmetry, because the magnitude of equilibrium deformations is usually small. By contrast, bending and twisting in a higher codimension can have a large effect on space group-dependent properties, for example, introducing a screw axis (as in a helix) modifies at least one translational symmetry. The effect of crystal symmetry on anisotropic material properties can be pronounced, as described in detail by Nye.[42] A classical example is that of birefringence, where symmetry breaking due to mechanical deformation can cause an isotropic material to show an anisotropic materials property. Using the terminology of Nye, *coupled effects* to deformation will be particularly affected. In thermoelastic systems, these properties include the heat of deformation, thermal expansion, piezocaloric effects, and thermal pressure. When other fields are considered, further properties include piezoelectricity and magnetostriction.

Codimension can also be used to understand more sophisticated nanostructure shapes that have a fractal character. Nanostructures such as polymer, nanotube, or nanowire networks can have a fractal dimension and therefore a noninteger codimension $c < 2$. We can contrast the properties of these fractal structures to those of linear, $c = 2$ structures. Such fractal nanostructures have, as a fundamental structural unit, point defects or branch/bifurcation points.[43] Examples of simple nanostructures containing such defects are X-, Y-, and T-shaped CNT junctions, which have recently been observed.[44] Composites reinforced with Y junctions have dramatically different strengths and toughnesses compared to those with straight nanotubes.[45,46] This suggests that the properties of fractal structures will be similarly affected compared to linear materials.

Although the concept of codimension-dependent properties was discussed in the context of nanostructures, it is general and applies to all low-dimensional systems that exhibit equilibrium shapes that are deformed relative to the common $c = 0$ case (i.e., $c > 0$). Two such examples are hippuric acid needles[47] and long leaves,[48] which respectively twist and bend during growth. Their properties should change similarly to our previously discussed examples. As a final note, we initially defined codimension as a fixed and integer value. As shown in the discussed examples, the effective codimension c_{eff} need not necessarily be an integer. In principle, it can be made to vary continually between two values. Properties can than be engineered by adjusting the values of the effective codimension.

VI. CONCLUSIONS

When materials are very thin in one or more dimensions, their equilibrium shape is often deformed (relative to the bulk material). This can be the result of, for example, surface stress, internal stress, piezoelectricity, and electrostatics. Because material properties are variations of

https://doi.org/10.1557/jmr.2011.306 Published online by Cambridge University Press

appropriate thermodynamic potentials from the *equilibrium* state, such *equilibrium* deformation may modify many material properties. Although these changes are profound for some properties, such as edge stress in graphene and the stiffness of a nanohelix, they have little effect on others, such as edge energy in graphene. For those properties that are sensitive to equilibrium deformation, their magnitude will be sensitive to the number of degrees of freedom that are accessed during deformation, that is, the codimension. This suggests new approaches to engineer nanomaterial properties.

ACKNOWLEDGMENTS

The authors gratefully acknowledge Prof. M. Haataja, Prof. Y.W. Zhang, Prof. S. Safran, Prof. C. Arnold, Dr. C.K. Gan, and Dr. C. Majidi for enlightening discussions and comments.

REFERENCES

1. S. Iijima: Helical microtubules of graphitic carbon. *Nature* **354**, 56 (1991).
2. H. Dai: Carbon nanotubes: Synthesis, integration, and properties. *Acc. Chem. Res*. **35**, 1035 (2002).
3. X. Duan and C.M. Lieber: General synthesis of compound semiconductor nanowires. *Adv. Mater*. **12**, 298 (2000).
4. Y. Wu, J. Xiang, C. Yang, W. Lu, and C.M. Lieber: Single-crystal metallic nanowires and metal/semiconductor nanowire heterostructures. *Nature* **430**, 61 (2004).
5. A.K. Geim and K.S. Novoselov: The rise of graphene. *Nat. Mater*. **6**, 183–191 (2007).
6. X.Y. Kong and Z.L. Wang: Spontaneous polarization-induced nanohelixes, nanosprings, and nanorings of piezoelectric nanobelts. *Nano Lett*. **3**, 1625–1631 (2003).
7. Z.W. Pan, Z.R. Dai, and Z.L. Wang: Nanobelts of semiconducting oxides. *Science* **291**, 1947–1949 (2001).
8. K.V. Bets and B.I. Yakobson: Spontaneous twist and intrinsic instabilities of pristine graphene nanoribbons. *Nano Res*. **2**, 161–166 (2009).
9. J.M. Garcia-Ruiz, E. Melero-Garcia, and S.T. Hyde: Morphogenesis of self-assembled nanocrystalline materials of barium carbonate and silica. *Science* **323**, 362–365 (2009).
10. M.H. Huang, C. Boone, M. Roberts, D.E. Savage, M.G. Lagally, N. Shaji, H. Qin, R. Blick, J.A. Nairn, and F. Liu: Nanomechanical architecture of strained bilayer thin films: From design principles to experimental fabrication. *Adv. Mater*. **17**, 2860–2864 (2005).
11. L. Zhang, E. Deckhardt, A. Weber, C. Schonenberger, and D. Grutzmacher: Controllable fabrication of SiGe/Si and SiGe/Si/Cr helical nanobelts. *Nanotechnology* **16**, 655–663 (2005).
12. M. Hazewinkel, Ed.: *Encyclopaedia of Mathematics;* Springer: New York; 1995.
13. *Encyclopaedia of mathematics:* http://eom.springer.de/C/c022870.htm (accessed August 11, 2011).
14. R. LeSar, R. Najafabadi, and D.J. Srolovitz: Thermodynamics of solid and liquid embedded-atom-method metals: A variational study. *J. Chem. Phys*. **94**, 5090–5097 (1991).
15. G.A. Mansoori and F.B. Canfield: Variational approach to melting. II. *J. Chem. Phys*. **51**, 4967–4972 (1969).
16. J. Steinmetz, S. Kwon, H.J. Lee, E. Abou-Hamad, R. Almairac, C. Goze-Bac, H. Kim, and Y.W. Park: Polymerization of conducting polymers inside carbon nanotubes. *Chem. Phys. Lett*. **431**, 139–144 (2006).
17. J. Steinmetz, H.J. Lee, S. Kwon, D.S. Lee, C. Goze-Bac, E. Abou-Hamad, H. Kim, and Y.W. Park: Routes to the synthesis of carbon nanotube–polyacetylene composites by Ziegler–Natta polymerization of acetylene inside carbon nanotubes. *Curr. Appl. Phys*. **7**, 39–41 (2007).
18. D. Nishide, T. Wakabayashi, T. Sugai, R. Kitaura, H. Kataura, Y. Achiba, and H. Shinohara: Raman spectroscopy of size-selected linear polyyne molecules C2NH2 ($n = 46$) encapsulated in single-wall carbon nanotubes. *J. Phys. Chem. C* **111**, 5178–5183 (2007).
19. A.V. Bazilevsky, K. Sun, A.L. Yarin, and C.M. Megaridis: Selective intercalation of polymers in carbon nanotubes. *Langmuir* **23**, 7451–7455 (2007).
20. G.C. McIntosh, D. Tománek, and Y.W. Park: Energetics and electronic structure of a polyacetylene chain contained in a carbon nanotube. *Phys. Rev. B* **67**, 125419 (2003).
21. W. Bao, F. Miao, Z. Chen, H. Zhang, W. Jang, C. Dames, and C.N. Lau: Controlled ripple texturing of suspended graphene and ultrathin graphite membranes. *Nat. Nanotechnol*. **4**, 562–566 (2009).
22. J.W. Jiang, J.S. Wang, and B.W. Li: Thermal expansion in single-walled carbon nanotubes and graphene: Nonequilibrium Green's function approach. *Phys. Rev. B* **80**, 205429 (2009).
23. D.Q. Zhang, A. Alkhateeb, H.M. Han, H. Mahmood, D.N. McIlroy, and M.G. Norton: Silicon carbide nanosprings. *Nano Lett*. **3**, 983–987 (2003).
24. A.M. Wahl: Helical compression and tension springs. *J. Appl. Mech*. **2**, A38 (1935).
25. C.J. Ancker, Jr. and J.N. Goodier: Pitch and curvature correction for helical springs. *J. Appl. Mech*. **25**, 466 (1958).
26. W. Young and R. Budynas: *Roark's Formulas for Stress & Strain*, 7th ed.; McGraw–Hill Professional: New York; 1984.
27. M.H. Gass, U. Bangert, A.L. Bleloch, P. Wang, R.R. Nair, and A.K. Geim: Free-standing graphene at atomic resolution. *Nat. Nanotechnol*. **3**, 676–681 (2008).
28. L. Tapaszto, G. Dobrik, P. Lambin, and L.P. Biro: Tailoring the atomic structure of graphene nanoribbons by scanning tunnelling microscope lithography. *Nat. Nanotechnol*. **3**, 397–401 (2008).
29. A.K. Geim: Graphene: Status and prospects. *Science* **324**, 1530–1534 (2009).
30. S. Jun: Density-functional study of edge stress in graphene. *Phys. Rev. B* **78**, 073405 (2008).
31. B. Huang, M. Liu, N.H. Su, J. Wu, W.H. Duan, B.L. Gu, and F. Liu: Quantum manifestations of graphene edge stress and edge instability: A first-principles study. *Phys. Rev. Lett*. **102**, 166404 (2009).
32. C.K. Gan and D.J. Srolovitz: Trends in graphene edge properties and flake shapes: A first-principles study. *Phys. Rev. B* **81**, 125445 (2010).
33. V.B. Shenoy, C.D. Reddy, A. Ramasubramaniam, and Y.W. Zhang: Edge-stress-induced warping of graphene sheets and nanoribbons. *Phys. Rev. Lett*. **101**, 245501 (2008).
34. F.G. Rammerstorfer, F.D. Fischer, and N. Friedl: Buckling of free infinite strips under residual stresses and global tension. *J. Appl. Mech*. **68**, 399–404 (2001).
35. Z.G. Chen, J. Zou, G. Liu, F. Li, Y. Wang, L. Wang, X.L. Yuan, T. Sekiguchi, H.M. Cheng, and G.Q. Lu: Novel boron nitride hollow nanoribbons. *ACS Nano* **2**, 2183–2191 (2008).
36. J. Campos-Delgado, J.M. Romo-Herrera, X. Jia, D.A. Cullen, H. Muramatsu, Y.A. Kim, T. Hayashi, Z. Ren, D.J. Smith, Y. Okuno, T. Ohba, H. Kanoh, K. Kaneko, M. Endo, H. Terrones, M.S. Dresselhaus, and M. Terrones: Bulk production of a new form of sp2 carbon: Crystalline graphene nanoribbons. *Nano Lett*. **8**, 2773–2778 (2008).

https://doi.org/10.1557/jmr.2011.306 Published online by Cambridge University Press

37. P.S. Branicio, C.K. Gan, M.H. Jhon, and D.J. Srolovitz: Properties on the edge: Graphene edge energies, edge stresses, edge warping, and the wulf shape of graphene flakes. *Model. Simul. Mater. Sci. Eng*. **19**, 054002 (2011).
38. D.W. Brenner, O.A. Shenderova, J.A. Harrison, S.J. Stuart, B. Ni, and S.B. Sinnott: A second-generation reactive empirical bond order (REBO) potential energy expression for hydrocarbons. *J. Phys.: Condens. Matter* **14**, 783–802 (2002).
39. Y. Liu, A. Dobrinsky, and B.I. Yakobson: Graphene edge from armchair to zigzag: The origins of nanotube chirality? *Phys. Rev. Lett*. **105**, 235502 (2010).
40. Q. Lu and R. Huang: Excess energy and deformation along free edges of graphene nanoribbons. *Phys. Rev. B* **81**, 155410 (2010).
41. G.H. Lui, L. Liu, K.F. Mak, G.W. Flynn, and T.F. Heinz: Ultraflat graphene. *Nature* **462**, 339–341 (2009).
42. J.F. Nye: *Physical Properties of Crystals: Their Representation by Tensors and Matrices;* Oxford University Press: Oxford, UK; 1984.
43. I.A. Ovid'ko: Nanodefects in nanostructures. *Phil. Mag. Lett*. **83**, 611–620 (2003).
44. M. Terrones, F. Banhart, N. Grobert, J.-C. Charlier, H. Terrones, and P.M. Ajayan: Molecular junctions by joining single-walled carbon nanotubes. *Phys. Rev. Lett*. **89**, 075505 (2002).
45. M.Y. Gutkin and I.A. Ovid'ko: Glide of hollow fibers at the bridging stage of fracture in ceramic nanocomposites. *Scripta Mater*. **59**, 414–417 (2008).
46. M.Y. Gutkin and I.A. Ovid'ko: Effect of y-junction nanotubes on strengthening of nanocomposites. *Scripta Mater*. **61**, 1149–1152 (2009).
47. A.G. Shtukenberg, J. Freudenthal, and B. Kahr: Reversible twisting during helical hippuric acid crystal growth. *J. Am. Chem. Soc*. **132**, 9341–9349 (2010).
48. H. Liang and L. Mahadevan: The shape of a long leaf. *Proc. Natl. Acad. Sci*. **106**, 22049–22054 (2009).
49. D.C. Liu and J. Nocedal: On the limited memory BFGS method for large-scale optimization. *Math. Program*. **45**, 503–528 (1989).

APPENDIX A: CALCULATION OF GRAPHENE EDGE ENERGY AND STRESS

GNR edge energy and stress are calculated in a similar manner as Jun[30] and Gan and Srolovitz.[32] The edge energy (per unit length) E_e as a function of edge orientation α is defined as

$$E_e(\alpha) = \frac{1}{2L}\left[E^N_{GNR}(\alpha) - NE_B\right] \quad , \qquad (A1)$$

where $E^N_{GNR}(\alpha)$ is the total energy of a GNR with N atoms, length L, and edge orientation α, and E_B is the energy per atom in a bulk (infinite) flat graphene sheet. The factor of 2 in the denominator of Eq. (A1) accounts for the fact that a GNR has two (parallel) edges. For narrow GNRs, $E_e(\alpha)$ depends on the GNR width because of interactions between the edges. This effect decays rapidly with GNR width. Therefore, we perform simulations on GNRs of widths in excess of 100 Å for which $E_e(\alpha)$ reaches the asymptotic value for large widths.

For all edge types, $E_e(\alpha)$ was calculated by minimizing the total energy with respect to all atomic coordinates at $T = 0$. We employed the limited-memory Broyden–Fletcher–Goldfarb–Shanno[49] method to relax the atomic structures (both in $c = 0$ and 1) until it converged to within 10^{-10} eV/atom. In the $c = 1$ case, noise was added to the initial atomic positions (i.e., perturbations in the atom positions from the flat structure) in order to break the symmetry of the problem.

We calculate the edge stress τ_e by straining the equilibrium (zero stress) GNR and interpolating the resultant system energy versus strain curve at $\epsilon = 0$. For $c = 0$, both compressive and tensile strains were employed, for $c = 1$, where the GNR buckles out of plane for compressive strains, only tensile strains were applied in order to determine τ_e.

https://doi.org/10.1557/jmr.2011.306 Published online by Cambridge University Press